



# Mechanisms of Interannual Variability of Ocean Bottom Pressure in the Southern Indian Ocean

Yuting Niu<sup>1,2</sup>, Xuhua Cheng<sup>1,2\*</sup>, Jianhuang Qin<sup>1,2</sup>, Niansen Ou<sup>3</sup>,  
Chengcheng Yang<sup>1,2</sup> and Duotian Huang<sup>1,2</sup>

<sup>1</sup> Key Laboratory of Marine Hazards Forecasting, Ministry of Natural Resources, Hohai University, Nanjing, China,

<sup>2</sup> College of Oceanography, Hohai University, Nanjing, China, <sup>3</sup> College of Ocean and Meteorology, Guangdong Ocean University, Zhanjiang, China

## OPEN ACCESS

### Edited by:

Fan Wang,  
Institute of Oceanology (CAS), China

### Reviewed by:

Jianing Wang,  
Institute of Oceanology (CAS), China  
Motoki Nagura,  
Japan Agency for Marine-Earth  
Science and Technology (JAMSTEC),  
Japan

### \*Correspondence:

Xuhua Cheng  
xuhua.cheng@hhu.edu.cn

### Specialty section:

This article was submitted to  
Physical Oceanography,  
a section of the journal  
Frontiers in Marine Science

Received: 09 April 2022

Accepted: 23 May 2022

Published: 15 June 2022

### Citation:

Niu Y, Cheng X, Qin J, Ou N,  
Yang C and Huang D (2022)  
Mechanisms of Interannual Variability  
of Ocean Bottom Pressure  
in the Southern Indian Ocean.  
Front. Mar. Sci. 9:916592.  
doi: 10.3389/fmars.2022.916592

The study of ocean bottom pressure (OBP) helps to understand the changes in the sea level budget and ocean deep circulation. In this study, the characteristics and mechanisms of interannual OBP variability in the Southern Indian Ocean are examined using Gravity Recovery and Climate Experiment (GRACE) satellite data from 2003 to 2016. Results show that there are two energetic OBP centers in the Southern Indian Ocean (50°–60°S, 40°–60°E and 45°–60°S, 80°–120°E). The OBP magnitudes at two centers have strong variability on interannual time scales, and their values are larger during austral summer (NDJF) and winter (JJAS). Atmospheric forcing plays an important role in local OBP variability. The high (low) sea level pressure (SLP) over the Southern Indian Ocean benefits positive (negative) OBP anomalies via the convergence (divergence) of Ekman transport driven by local wind. Such SLP anomalies are related to the Southern Annular Mode (SAM), Southern Oscillation (SO) and Indian Ocean dipole (IOD). SAM can influence the OBP changes in both austral summer and winter, while SO and IOD have positive correlations with OBP variability during austral summer and austral winter, respectively. These results are validated by a mass-conservation ocean model, which further confirms the importance of atmospheric forcing on the interannual OBP variations.

**Keywords:** ocean bottom pressure, Southern Indian Ocean, wind forcing, sea level pressure anomaly, Ekman transport

## 1 INTRODUCTION

The fluctuations in gravity field intensity reflect the mass distribution in the ocean, atmosphere, solid earth and the storage of water, snow and ice on land (Dickey et al., 1997). On seasonal to interannual time scales, changes in the gravity field can be considered as the changes in a thin layer of water covering the Earth's surface, which is equivalent to the ocean bottom pressure (OBP) in the ocean (Hughes et al., 2000). Actually, the variability of OBP is the changes in ocean and atmospheric mass acting on the unit area of the seabed (usually translated into equivalent changes in sea level), which includes atmospheric information and ocean responses. As one of the major components of sea level variability, the OBP change is related to the ocean mass change, which contributes to approximately 60% of the global mean sea level rise (Chambers et al., 2017; Cazenave et al., 2018).

Therefore, insight into the variability of the OBP is expected to benefit the diagnosis of changes in sea level budget (Chambers, 2011; Cheng et al., 2013), water cycle (Landerer and Swenson, 2012), global energy budget (Johnson and Chambers, 2013), ocean circulation (Hughes and de Cuevas, 2001; Makowski et al., 2015) and other aspects of climate change.

The Southern Ocean plays a central role in the global meridional overturning circulation, global climate system, carbon cycle, and sea level rise (Rintoul, 2018). However, it has always been an under sampled area in the world's oceans. As a result, studies of OBP in the Southern Ocean were based on theoretical derivations, numerical simulations or local observations before the 21st century (e.g., Gill and Niiler, 1973; Hughes and Smithson, 1996; Woodworth et al., 1996; Ponte, 1999). After the launch of the Gravity Recovery and Climate Experiment (GRACE) satellite in 2002, a new era of high precision and long-term continuous direct observation of OBP on a global scale emerged. GRACE provides large amounts of high-quality data for OBP studies in the Southern Ocean (Tapley et al., 2004; Chambers and Willis, 2009; Jin, 2013; Tapley et al., 2019). The most significant seasonal variations in the OBP usually occur at high latitudes of the Southern Ocean, and the amplitude of seasonal signals is typically 4–5 cm root mean square (Peralta-ferriz et al., 2017; Cheng et al., 2021). GRACE data show that the variability of OBP from sub-seasonal to interannual time scales is consistent with the variability of high latitude sea level in the South Pacific, South Atlantic and South Indian Ocean (e.g., Kanzow et al., 2005; Johnson and Chambers, 2013; Piecuch et al., 2013; Ponte and Piecuch, 2014). Chambers and Willis (2009) noted that the regional OBP has a close relationship with the exchanges of mass on sub-seasonal and interannual time scales.

The local OBP variability is commonly induced by local mass redistribution, which is mainly associated with wind-driven ocean circulation and represents the barotropic response of ocean to the changes of wind stress (Gill and Niiler, 1973). The contribution of baroclinic processes to OBP is much weak in the deep ocean at high latitudes (Piecuch and Ponte, 2014). Based on GRACE observations and numerical models, some studies discussed the wind-induced OBP in the Southern Ocean. For instance, Cabanes et al. (2006) suggested that the local Sverdrup transport and Ekman pumping driven by the local wind stress are important factors for sea level rise and OBP variability in the South Atlantic. Boening et al. (2011) revealed that the observed high OBP signal in the Southeast Pacific at the end of 2009 are associated with the reinforcement of the topographic effect by the anticyclonic wind anomalies. Ponte and Piecuch (2014) demonstrated the role of local wind stress curl on OBP in the Southeast Indian Ocean and the Southeast Pacific which is consistent with Gill and Niiler (1973). The trend of OBP in the Southern Indian Ocean and Southern Atlantic is also closely related to winds (Makowski et al., 2015). In addition to winds, the hydrological cycle (Chambers et al., 2004), atmospheric pressure over the ocean (Ponte, 1999; Cheng et al., 2021) and baroclinic processes (Huang and Jin, 2002; Piecuch et al., 2013; Piecuch and Ponte, 2014) also accounts for the OBP variations to

some extent, but the wind forcing plays the dominate role in OBP variation at mid-high latitudes on sub-seasonal to interannual timescales.

Wind forcing is commonly linked to atmospheric teleconnections, such as Southern Annular Mode (SAM) and El Niño-Southern Oscillation (ENSO). Previous studies have reported the high correlation between SAM and OBP in the Southern Ocean (e.g., Ponte and Piecuch, 2014; Makowski et al., 2015). Moreover, it is well known that ENSO extends its influence beyond the tropical Pacific through atmospheric teleconnection (Alexander et al., 2002; Yeh et al., 2009), thus the variability of OBP in the South Pacific can be influenced by ENSO (Lee et al., 2010; Boening et al., 2011; Qin et al., 2022).

Previous studies suggested that the wind forcing plays an important role in the interannual variability of OBP based on a relatively short period data or case studies (e.g., Gill and Niiler, 1973; Makowski et al., 2015; Cheng et al., 2021). As the length of the data extends, the significance of correlation between wind forcing and OBP variations needs further examination using long period data. So far, the role of atmospheric teleconnections in surface wind anomalies in the Southern Indian Ocean also has less been investigated. In addition, a mass-conserving model is applied to explore the mechanism of OBP variability in this study, which is more suitable to study OBP and sea level variability (Huang et al., 2001). Overall, the mechanism of OBP variability in the Southern Indian Ocean, especially its relationship with atmospheric teleconnection, still remains an interesting issue. In this study, the interannual variability of OBP in the Southern Indian Ocean associated with atmospheric teleconnections is investigated using GRACE data and a mass-conserving model. The remainder of this paper is organized as follows. The data, model and methods in this study are introduced in Section 2. The characteristics and mechanisms of OBP variability are examined in Section 3. Finally, Section 4 shows a summary and discussion.

## 2 DATA AND METHODS

The gridded monthly GRACE OBP data ( $1^\circ \times 1^\circ$ ), derived from the Center for Space Research (CSR) of the University of Texas for Space Research Release 06 (RL06) solutions, spanning from 2003 to 2016, are available from [http://www2.csr.utexas.edu/grace/RL06\\_mascons.html/](http://www2.csr.utexas.edu/grace/RL06_mascons.html/). Compared to the RL05 version, RL06 mascon solutions use a newly defined grid to minimize the leakage between land and ocean signals. The Atmospheric pressure has been removed. Besides, we use the linear interpolation method to reconstruct the values in months to avoid missing values. Atmospheric variables including sea level pressure (SLP), sea surface temperature (SST), winds and 200 hPa geopotential height are obtained from ERA5 monthly averaged data, which are provided by the European Centre for Medium-Range Weather Forecasts (ECMWF), <https://cds.climate.copernicus.eu/cdsapp#!/dataset/reanalysis-era5-single-levels-monthly-means?tab=form/>), with a resolution of  $0.25^\circ \times 0.25^\circ$  for the period of 2003–2016.

The monthly sea level anomaly (SLA) data used in this study was released by the European Copernicus Marine Environment Monitoring Service (CMEMS, <https://marine.copernicus.eu>). The data are available on a  $1/4^\circ$  Mercator grid at monthly intervals and spans a period from 2003 to 2016. To calculate the steric sea level, we use monthly temperature and salinity data for 2003–2016 from global ocean Argo grid dataset (BOA-Argo, <http://www.argo.org.cn/>). The product has a  $1^\circ \times 1^\circ$  horizontal resolution and 58 vertical levels from sea surface to 2000 m depth.

The SAM index (SAMI) is defined as the difference of the normalized zonal mean SLP of  $40^\circ$ – $65^\circ$ S (Marshall, 2003), which is downloaded from <https://legacy.bas.ac.uk/met/gjma/sam.html>. The Southern Oscillation Index (SOI) is used as the ENSO index, which is available from [https://psl.noaa.gov/gcos\\_wgsp/Timeseries/SOI/](https://psl.noaa.gov/gcos_wgsp/Timeseries/SOI/). The dipole mode index (DMI) is used as the Indian Ocean Dipole (IOD) index, which can be downloaded from [https://psl.noaa.gov/gcos\\_wgsp/Timeseries/Data/dmi.long.data](https://psl.noaa.gov/gcos_wgsp/Timeseries/Data/dmi.long.data).

A pressure coordinate ocean model (PCOM) based on mass conservation is used in this study, which was developed by Huang et al. (2001) and improved by Zhang et al. (2014). Since PCOM is a truly compressible ocean model (i.e., free of the Boussinesq approximation), it can provide more accurate simulations of OBP than Boussinesq approximation models. The model is first spun-up for 600 years from a static state under repeating climatological monthly mean atmospheric forcing, including fresh water flux, surface heat flux, surface wind and SLP. Then, two experiments that start from the spin-up run are used to verify the mechanisms of OBP variability in the Southern Indian Ocean in this study. The control run (Exp.1) is forced by daily atmospheric forcing over 1990–2018. Exp. 2 is a similar experiment without wind forcing. This model has a horizontal resolution of  $1^\circ \times 1^\circ$ , with 60 pressure layers. The model has been successfully applied to the studies of OBP variations in the global and regional oceans (Cheng et al., 2021; Qin et al., 2022). To quantify the contribution of wind forcing to OBP, two idealized PCOM experiment are designed, which are forced by the regression wind anomalies.

Wind stress alters the mass distribution of sea water via changing Ekman transport. The zonal and meridional Ekman transports are calculated from Price et al. (1987):

$$U_E = \frac{\tau^{(y)}}{\rho f} \quad (1)$$

$$V_E = -\frac{\tau^{(x)}}{\rho f} \quad (2)$$

where  $\tau^{(x)}$  and  $\tau^{(y)}$  are the surface wind stresses  $\rho$  is the seawater density, which is assumed constant at  $1025 \text{ kg/m}^3$ ;  $f$  is the Coriolis parameter.

In this study, we calculated the monthly anomalies by removing the climatological annual cycle and trends of the original data. The austral summer covers NDJF (November–February), and the austral winter is defined as JJAS (June–

September). The regression method we adopted is unitary linear regression. The Student's *t-test* is used to test the statistical significance of correlation coefficients and regression coefficients.

### 3 RESULTS

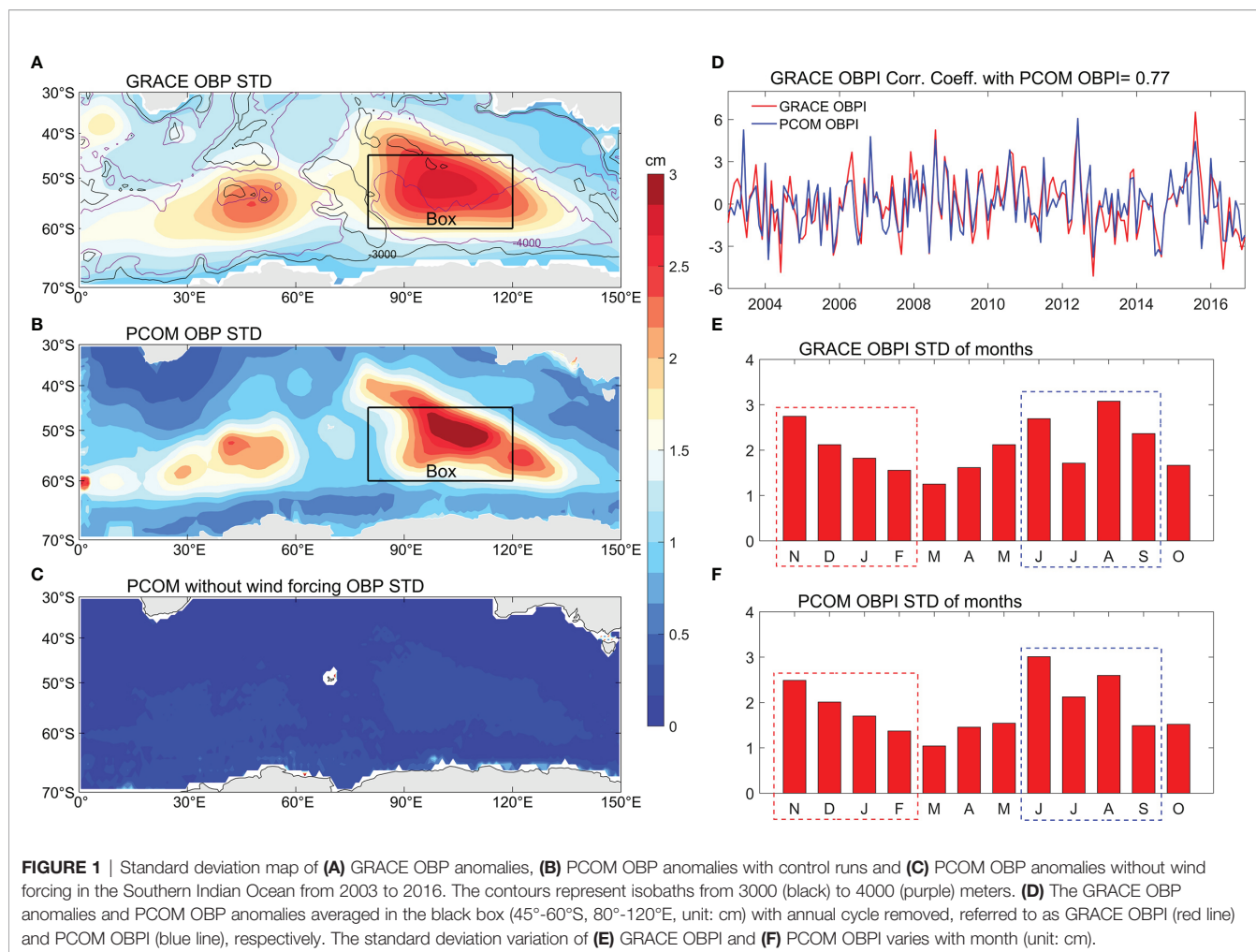
#### 3.1 Characteristics of OBP Variability in the Southern Indian Ocean

The standard deviation maps of monthly GRACE OBP and PCOM OBP (Exp.1) from 2003 to 2016 are shown in **Figures 1A, B**, respectively. There are two energetic OBP centers with maximum values higher than 2.5 cm in the Southern Indian Ocean in both GRACE and PCOM control runs. This result is consistent with Jin (2013) and Ponte and Piecuch (2014), who reported the large variability of OBP there. In contrast, these two energetic OBP centers are very weak in the PCOM solution without wind forcing (**Figure 1C**), which indicates that active OBP centers in the Southern Indian Ocean are mainly forced by wind.

The OBP anomalies averaged in the region ( $45^\circ$ – $60^\circ$ S,  $80^\circ$ – $120^\circ$ E; black box in **Figure 1A**) is considered as an index that measures the variability of the OBP in the Southern Indian Ocean. The OBP indices in the GRACE and PCOM control runs (hereafter referred to as the GRACE OBPI and PCOM OBPI, respectively) are shown in **Figure 1D**. The correlation coefficient between two OBPIs is 0.77 (significant at the 99% confidence level), and both GRACE OBPI and PCOM OBPI have a maximum amplitude above 6 cm. According to the monthly standard deviation of the GRACE OBPI and PCOM OBPI (**Figures 1E, F**), one can see that although the climatological annual cycle has been removed, they are relatively active during austral summer (NDJF) and winter (JJAS).

**Figure 2** shows the empirical orthogonal function (EOF) analysis of monthly GRACE OBP anomalies in the Southern Indian Ocean ( $30^\circ$ – $70^\circ$ S,  $20^\circ$ – $130^\circ$ E). EOF1 and EOF2 account for 42.8% and 15.6% of the total variance, respectively. The spatial structure of EOF1 is similar to the standard deviation map of the OBP in the Southern Indian Ocean (**Figure 1A**), and its corresponding principal component (PC) is closely related to the GRACE OBPI and PCOM OBPI ( $R = 0.94$  and  $0.72$ , respectively, both of which are significant at the 99% confidence level) during the period of 2003–2016. The spatial structure of EOF2 shows a dipole mode in the zonal direction, but the correlation coefficient between PC2 and GRACE OBPI is only 0.31, and that with PCOM OBPI is 0.22 (respectively, not significant at the 95% confidence level). Thus, the OBPI can be used to represent the temporal variations of EOF1 in both GRACE and PCOM control runs.

**Figure 3** shows the regression maps of OBP anomalies and Ekman transports upon the normalized OBPI in the GRACE and PCOM control runs during summer (NDJF) and winter (JJAS), when the OBP variations are active. The positive OBP in the Southern Indian Ocean is obviously accompanied by convergence of Ekman transport, which is consistent with



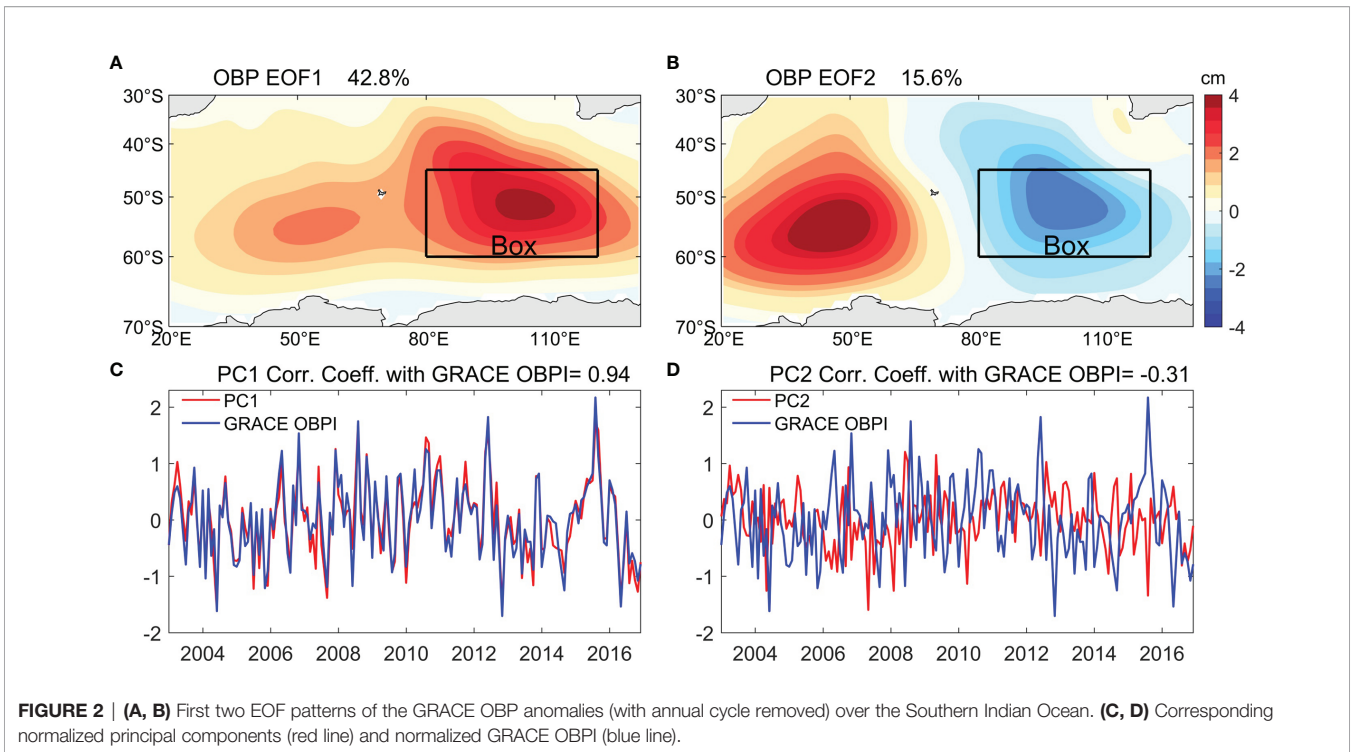
previous findings (Gill and Niiler, 1973; Jing and Cheng, 2019; Cheng et al., 2021). It emphasizes the atmospheric source for the variability of OBP in the Southern Indian Ocean, which has not been well investigated in previous studies. Thus, the following study is focused on the possible source of wind forcing for the active OBP in the Southern Indian Ocean during summer (NDJF) and winter (JJAS).

### 3.2 Mechanisms of OBP Variability During Austral Summer and Winter

The regression maps of SLP anomalies and 10 m winds upon the normalized GRACE OBPI during summer (NDJF) and winter (JJAS) are shown in **Figures 4A, C**, respectively. There is a significant closed high pressure over the Southern Indian Ocean during both austral summer and winter. The anticyclone associated with anti-clockwise winds is favorable for convergence of Ekman transports there, which leads to enhanced OBP anomalies. Conversely, the SLP anomaly shows negative values to the south of  $60^{\circ}$ S and positive values around mid-latitudes. This result indicates the influence of the sea-saw pattern of SLP on the variability of the OBP in the Southern Indian Ocean, especially during austral summer (NDJF; **Figure 4A**), which is similar to the

positive phase of SAM. Similar results are observed in the PCOM control runs (**Figures 4B, D**). To quantify the contribution of wind forcing to OBP, two idealized PCOM experiments are used (**Figure 5**). The experiments are forced by the regression wind anomalies (vectors in **Figures 4A, C**). The OBP anomalies diagnosed by PCOM are comparable to the regression maps (**Figure 3**). The results suggest that the wind anomalies are strong enough to trigger the interannual OBP variations in the Southern Indian Ocean.

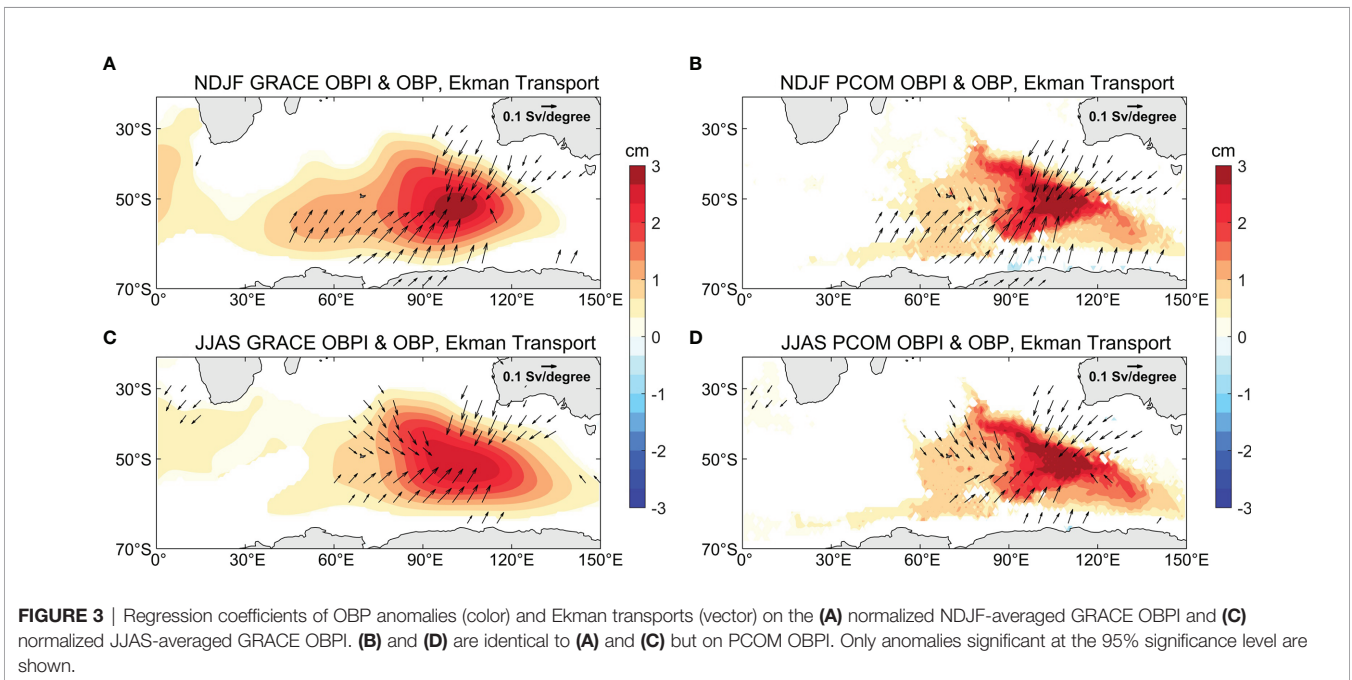
The correlation coefficients of the NDJF-averaged SAMI with concurrent GRACE OBPI and PCOM OBPI are 0.83 and 0.65 (**Figure 6**), respectively. The correlation between SAMI and OBP indices is also high during austral winter (JJAS;  $R = 0.69$  and  $0.64$ ). All correlation coefficients are significant at the 95% confidence level, which suggests the crucial impacts of SAM on the simultaneous variability of OBP in the Southern Indian Ocean (black lines in **Figure 6**). The regression results of SLP anomalies, 10 m winds, OBP anomalies and Ekman transports on the normalized SAMI during summer (NDJF) and winter (JJAS) are shown in **Figures 7A–D**. As shown in **Figures 7A, C**, SAM can stimulate a high-pressure anomaly in the Southern Indian Ocean (approximately  $45^{\circ}$ S,  $90^{\circ}$ E), which contributes to the wind-driven

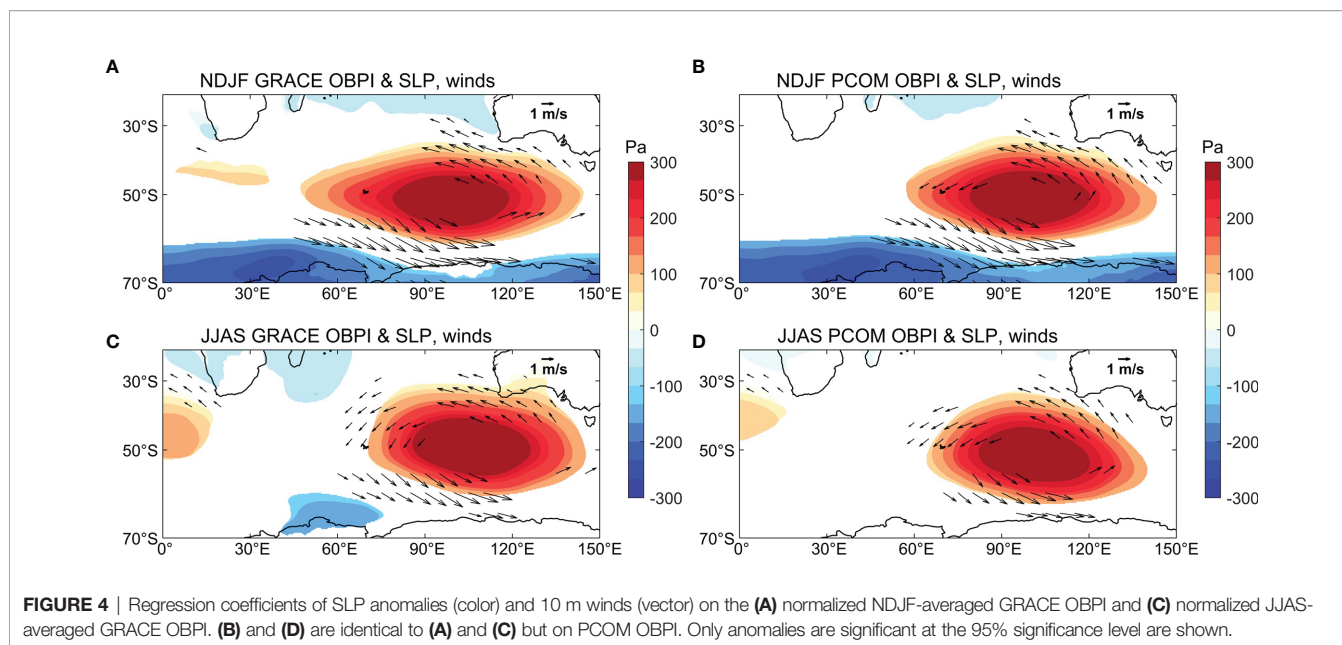


convergence Ekman transport. As a result, both austral summer (NDJF) and winter (JJAS) OBP anomalies are enhanced in the Southern Indian Ocean during positive phase of SAM.

Since some studies have suggested the influence of the tropics on SLP anomalies in the Southern Hemisphere (e.g. Ding et al., 2012), the lead correlation method is used to further determine the origin of OBP variability from the tropics. Due to the strong interannual

variability of ENSO and IOD, the correlations between their indices and OBPI are checked. The correlation coefficients between 4-month running mean SAMI, SOI, DMI and the NDJF-averaged GRACE OBPI are shown in **Figures 6A, B**. One can see that the correlation coefficient of the GRACE OBPI with SOI is highest ( $R = 0.56$ , significant at the 95% confidence level) during austral summer (NDJF), but not significant during austral winter (JJAS).



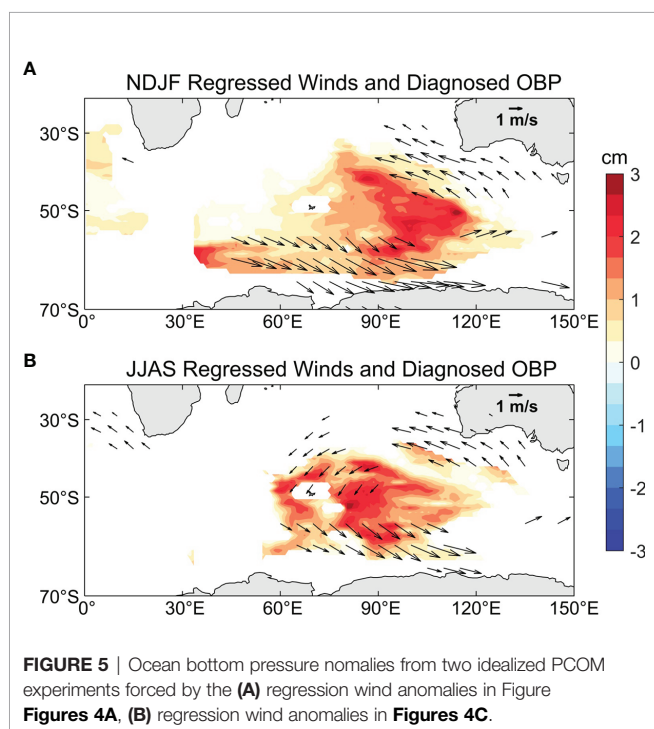


Additionally, the DMI can lead the JJAS-averaged GRACE OBPI by approximately 2 months with the highest correlation coefficient of 0.68 (significant at the 95% confidence level).

Such different results during summer (NDJF) and winter (JJAS) are mainly attributed to the seasonal phase lock of ENSO and IOD. The SLP anomalies associated with the Southern Oscillation (SO) have seasonal variability and show a positive center over the Southern Indian Ocean during austral summer (NDJF; Figures 7E, 8A–C). This result is consistent with Taschetto et al. (2011), who reported high pressure over the Southern Indian Ocean

during ENSO. To further investigate the dynamical mechanism, we checked the regression of zonal mean vertical wind anomalies of 90°–120°E on the normalized NDJF-averaged SOI (Figure 9). We find that the positive phase of SO can cause an updraft in the tropics and downdraft in the extra-tropics, leading to an anomalous anticyclonic air circulation over the study area during austral summer. It benefits the convergence of Ekman transport and intensified the OBP there (Figure 7F). On the other hand, a positive IOD features an anomalously strong west–east SST gradient in the tropical Indian Ocean, and the SST signal can last until SON. Meanwhile, the SST-induced air convection stimulates a Rossby wave train at 200 hPa transferring from the tropical Indian Ocean to emanate poleward and eastward of the Southern Indian Ocean (Figures 10A, B), which is beneficial to the generation of an anomalous anticyclone in our study area (Figures 10C, 7G), resulting in the increase of OBP during austral winter (JJAS; Figure 7H). This result is consistent with McIntosh and Hendon (2018), who mentioned the specific path of the Rossby wave train and the high pressure anomalies in our study area. Therefore, SO plays an important role in OBP variability in the Southern Indian Ocean during austral summer (NDJF), while the IOD mode is crucial during austral winter (JJAS). Such results can also be reproduced by PCOM, which are not shown.

Besides wind forcing, strong OBP centers are also related to closed planetary potential vorticity (i.e.,  $f/H$  with  $f$  being the Coriolis parameter and  $H$  the depth of the ocean) contours. There are closed planetary potential vorticity contours on the east and west sides of the Southern Indian Ocean (Figure 11), which can prevent the OBP signals from propagating outside the deep basin (Gill and Niiler, 1973; Cheng et al., 2021). Similar to the definition of OBPI, a simple index calculated with the OBP anomalies averaged in the southwestern Indian Ocean (50°–60°S, 40°–60°E) is named as OBPI-W. Figure 12 shows the regression maps of OBP anomalies, Ekman transports, SLP anomalies and 10 m winds on the normalized OBPI-W in the GRACE and PCOM control runs.



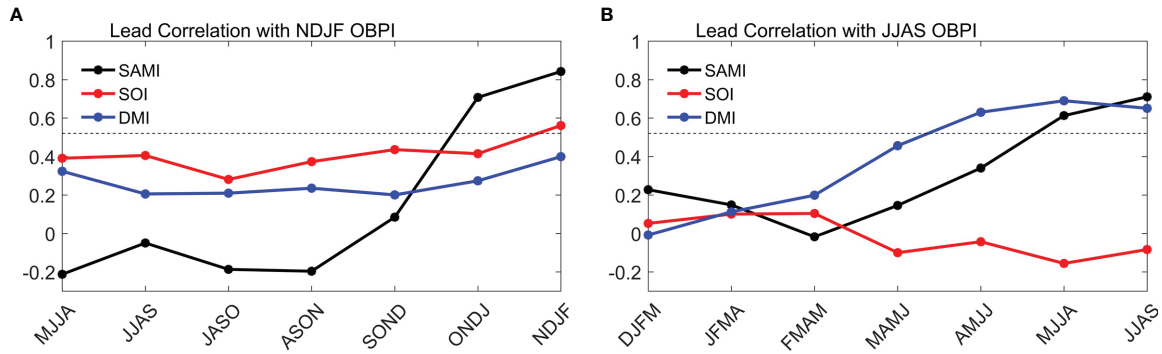


**FIGURE 6** | Lead correlation coefficients of the (A) NDJF-averaged GRACE OBPI and (B) JJAS-averaged GRACE OBPI with the 4-month averaged SAMI, SOI and DMI. The horizontal dashed line shows the 95% significance level.

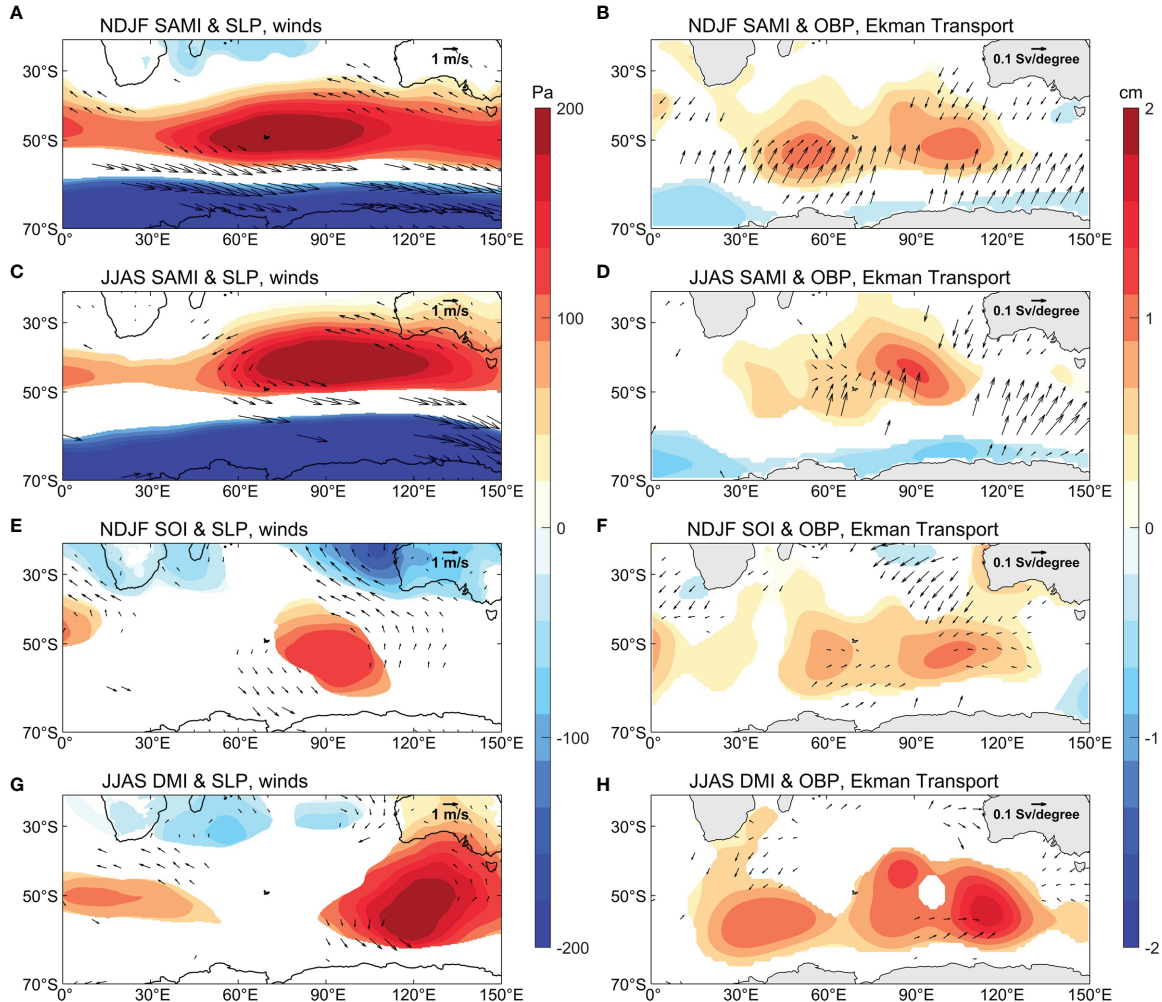
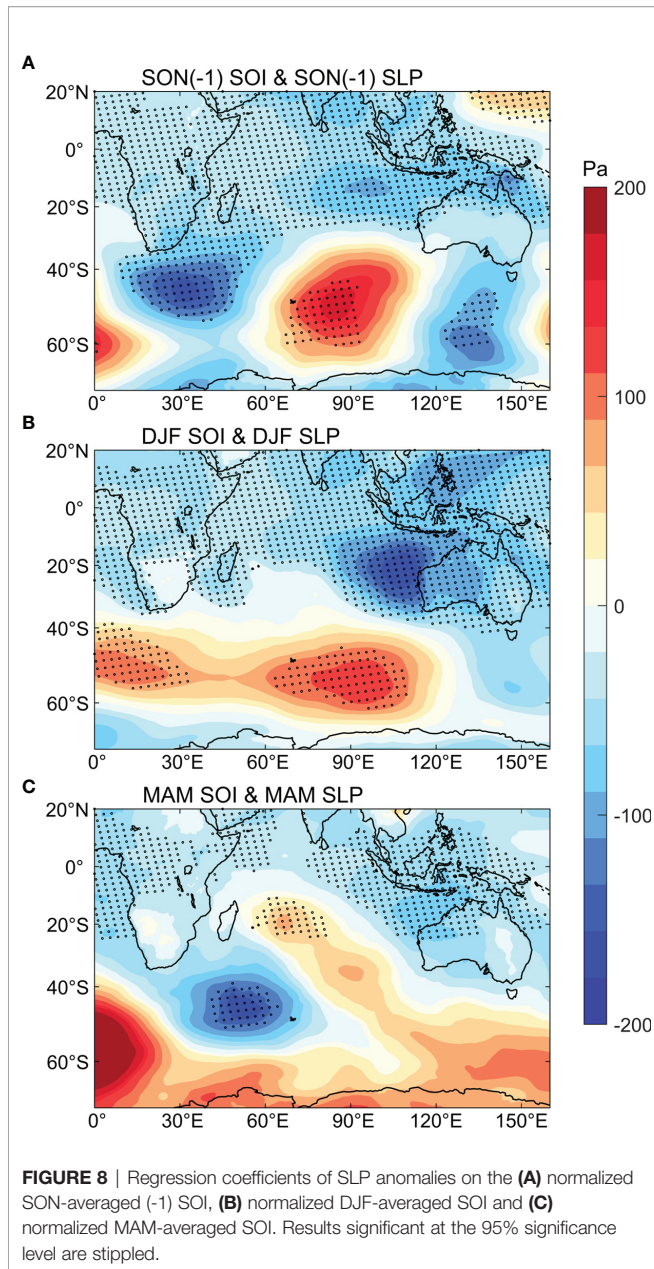


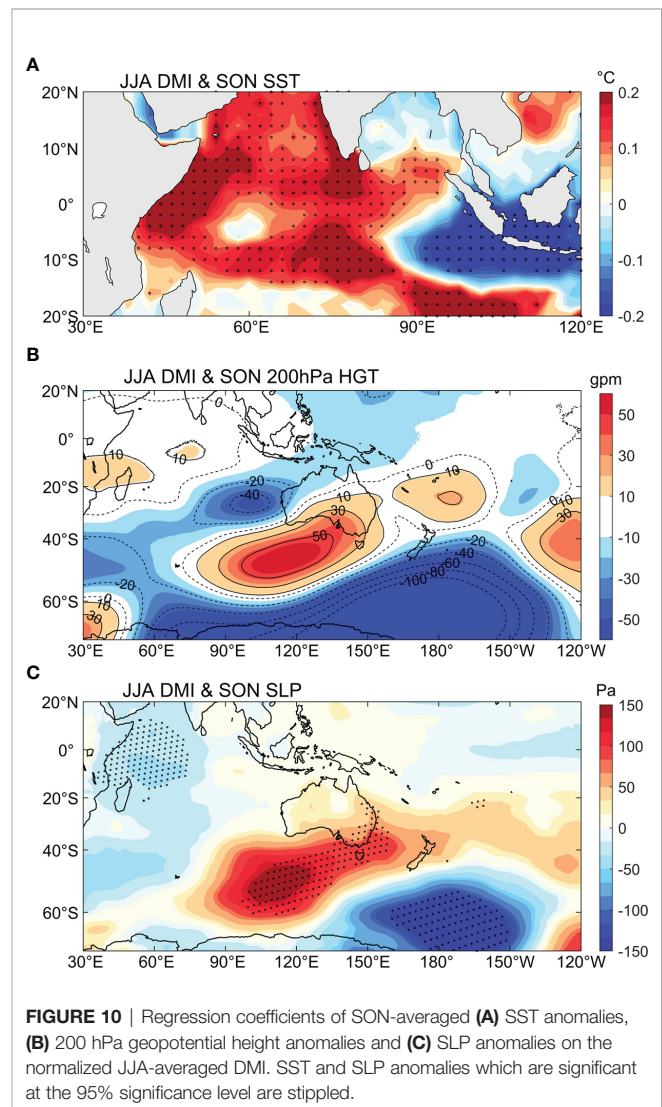
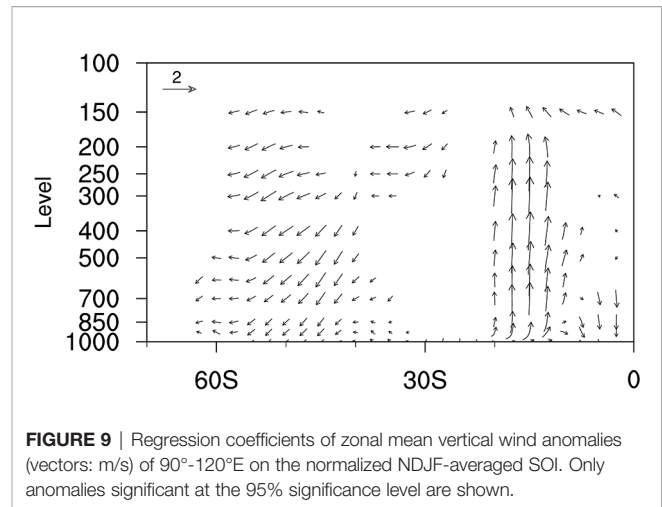
**FIGURE 7** | Regression coefficients of SLP anomalies (color) and 10 m winds (vector) on the (A) normalized NDJF-averaged SAMI, (C) normalized JJAS-averaged SAMI, (E) normalized NDJF-averaged SOI and (G) normalized JJAS-averaged DMI. (B, D, F, H) are identical to (A, C, E, G) but for OBP anomalies (color) and Ekman transports (vector). Only anomalies significant at the 95% significance level are shown.



Results show that the western energetic OBP center is also related to the wind anomalies caused by the SLP anomalies. Further analysis suggests that the OBP variability in the southwestern Indian Ocean is closely related to SAM, which can be seen from **Figures 7A–D** and it is weakly related to ENSO and IOD. SAM can explain 36% variation of OBP on interannual time scales, with the exception of IOD and ENSO (not shown).

### 4 CONCLUSIONS AND DISCUSSION

Using the GRACE observations and PCOM output, the characteristics and mechanisms of OBP variability in the Southern Indian Ocean on an interannual time scales are



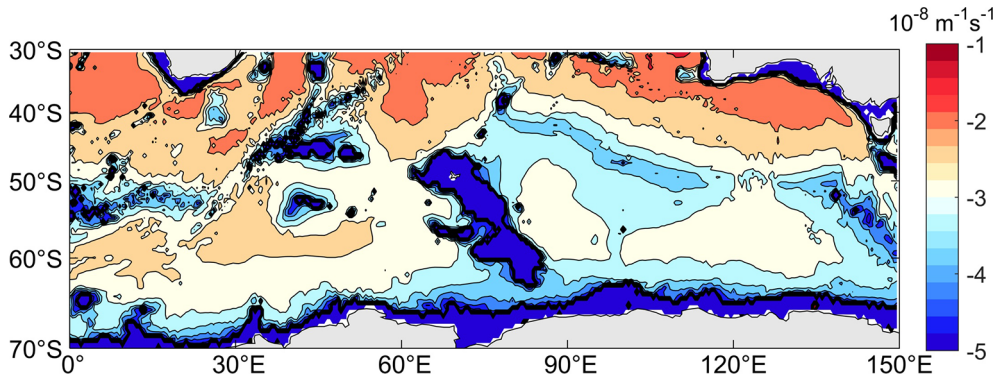


**FIGURE 11** | Absolute value of planetary potential vorticity in the Southern Indian Ocean.

investigated in this study. There are two energetic OBP centers in the Southern Indian Ocean, the OBP anomalies averaged in the eastern center is considered as an index (OBPI) to measure the OBP variations, which is highly correlated with the PC of the OBP EOF1 (variance contribution is 42.8%). It can be found that OBP in the Southern Indian Ocean has significant interannual variability and is more active during austral summer (NDJF) and winter (JJAS). In addition to the effect of topography, wind forcing plays a dominant role in OBP variability by changing the local Ekman transport, which is consistent with previous studies (e.g., Gill and Niiler, 1973; Jing and Cheng, 2019; Cheng et al., 2021). The closed anticyclone associated with clockwise winds benefits the convergence of Ekman transport and enhances local OBP anomalies.

Our study preliminarily discussed the possible atmospheric sources of anticyclone anomalies in the Southern Indian Ocean.

We find that the SLP anomalies are related to SAM, SO and IOD on interannual time scales. SAM can affect the OBP variability during the entire year, while SO and IOD only positively affect the OBP variability during austral winter (NDJF) and austral summer (JJAS), respectively. The positive phase of SO can cause an updraft in the tropics and downdraft in the extra-tropics, leading to an anomalous anticyclonic air circulation over the study area during austral summer. The SST-induced air convection associated with the positive phase of IOD forces a Rossby wave train transferring from tropical Indian Ocean to the south of Australia, resulting in an anomalous anticyclone appears in the Southeast Indian Ocean during austral winter.

In general, the results in this study help to understand the potential mechanisms of OBP fluctuations in the Southern Indian Ocean on interannual time scales. In this region, changes in OBP dominate the variations of sea level on

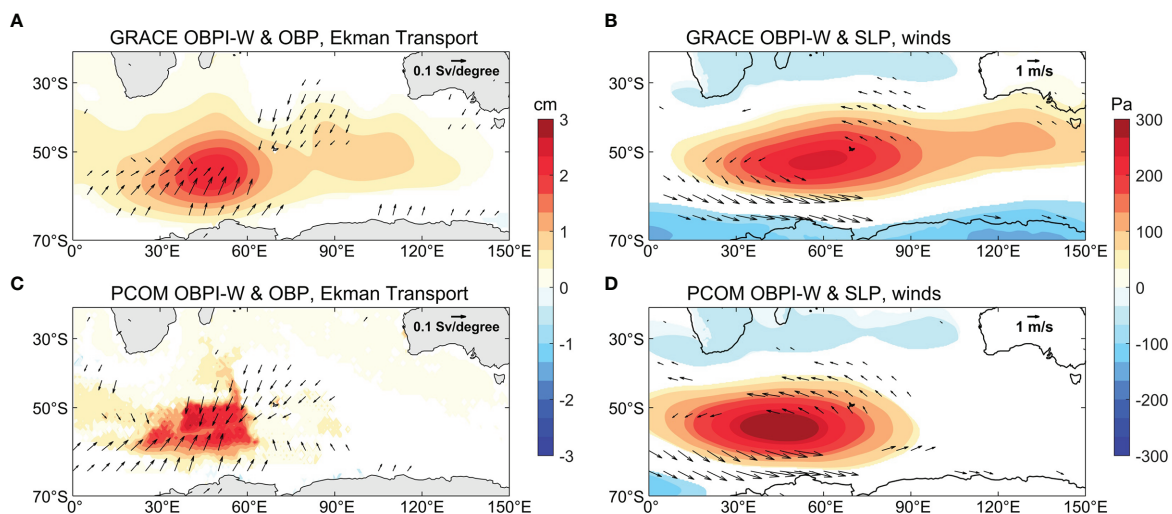
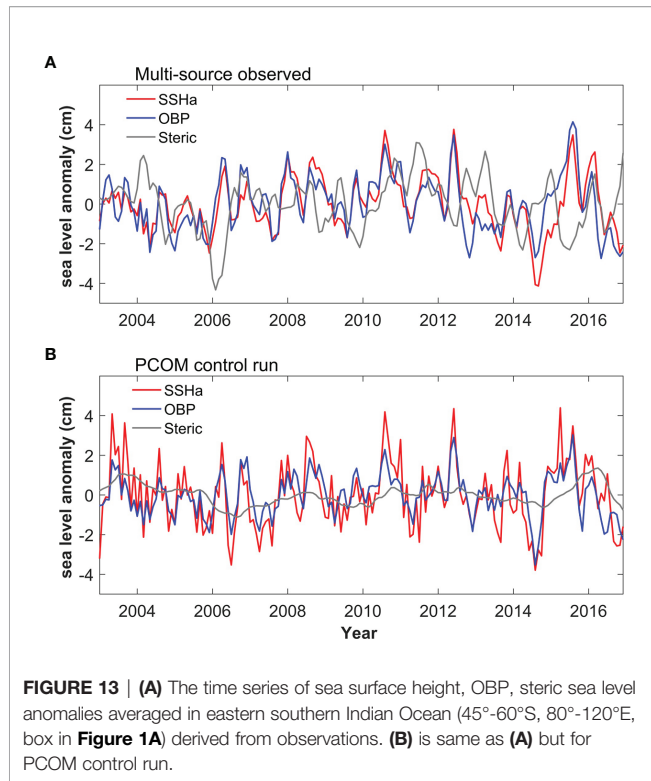


**FIGURE 12** | Regression coefficients of OBP anomalies (color) and Ekman transports (vector) on the (A) normalized GRACE OBPI-W and (C) normalized PCOM OBPI-W. (B, D) are identical to (A, C) but for SLP anomalies (color) and 10 m winds (vector). Only anomalies that are significant at the 95% significance level are shown.



interannual time scales (**Figure 13**). The correlation coefficient between observed sea level anomaly and OBP anomaly is 0.79 (significant at the 95% confidence level). Very good coherence also exists between them in the PCOM. Therefore, the study of OBP also can improve the understanding of the dynamics of sea level variations in Southern Indian Ocean.

To date, the time series of GRACE satellite data is not sufficiently long for interdecadal analysis and long-term

correlation between OBP variability and climate modes. Considering the important role of OBP in sea level change, long-term series observation data are of great significance for exploring the OBP mechanisms and predicting the sea level rise. PCOM well reproduces the observed OBP variations, because the wind forcing plays a crucial role in interannual variations of OBP in the Southern Ocean. To study the long-term change of OBP, the model must be further improved to include the effects of glaciers and rivers, which could improve the performance of the model to simulate and predict the impact of regional OBP variability on the global sea level rise.

## DATA AVAILABILITY STATEMENT

The original contributions presented in the study are included in the article/supplementary material. Further inquiries can be directed to the corresponding author.

## AUTHOR CONTRIBUTIONS

XC initiated the idea of this study. YN and XC wrote the manuscript. Other authors contributed to the data analysis and running the PCOM model. All authors contributed to the article and approved the submitted version.

## FUNDING

This research was supported by the National Key R&D Program of China (2018YFA0605702) and the Natural Science Foundation of China (Grant nos. 41522601, 41876002, 41876224).

## REFERENCES

- Alexander, M. A., Bladé, I., Newman, M., Lanzante, J. R., Lau, N. C., and Scott, J. D. (2002). The Atmospheric Bridge: The Influence of ENSO Teleconnections on Air-Sea Interaction Over the Global Oceans. *J. Clim.* 15, 2205–2231. doi: 10.1175/1520-0442(2002)015<2205:TABTIO>2.0.CO;2
- Boening, C., Lee, T., and Zlotnicki, V. (2011). A Record-High Ocean Bottom Pressure in the South Pacific Observed by GRACE. *Geophys. Res. Lett.* 38, 2–7. doi: 10.1029/2010GL046013
- Cabanes, C., Huck, T., and Colin de Verdière, A. (2006). Contributions of Wind Forcing and Surface Heating to Interannual Sea Level Variations in the Atlantic Ocean. *J. Phys. Oceanogr.* 36, 1739–1750. doi: 10.1175/JPO2935.1
- Cazenave, A., Meyssignac, B., Ablain, M., Balmaseda, M., Bamber, J., Barletta, V., et al. (2018). Global Sea-Level Budget 1993–Present. *Earth Syst. Sci. Data* 10, 1551–1590. doi: 10.5194/essd-10-1551-2018
- Chambers, D. P. (2011). ENSO-Correlated Fluctuations in Ocean Bottom Pressure and Wind-Stress Curl in the North Pacific. *Ocean. Sci.* 7, 685–692. doi: 10.5194/os-7-685-2011
- Chambers, D. P., Cazenave, A., Champollion, N., Dieng, H., Llovel, W., Forsberg, R., et al. (2017). Evaluation of the Global Mean Sea Level Budget Between 1993 and 2014. *Surv. Geophys.* 38, 309–327. doi: 10.1007/s10712-016-9381-3
- Chambers, D. P., Wahr, J., and Nerem, R. S. (2004). Preliminary Observations of Global Ocean Mass Variations With GRACE. *Geophys. Res. Lett.* 31, 1–4. doi: 10.1029/2004GL020461
- Chambers, D. P., and Willis, J. K. (2009). Low-Frequency Exchange of Mass Between Ocean Basins. *J. Geophys. Res. Ocean.* 114, 1–10. doi: 10.1029/2009JC005518
- Cheng, X., Li, L., Du, Y., Wang, J., and Huang, R. X. (2013). Mass-Induced Sea Level Change in the Northwestern North Pacific and its Contribution to Total Sea Level Change. *Geophys. Res. Lett.* 40, 3975–3980. doi: 10.1002/grl.50748
- Cheng, X., Ou, N., Chen, J., and Huang, R. X. (2021). On the Seasonal Variations of Ocean Bottom Pressure in the World Oceans. *Geosci. Lett.* 8. doi: 10.1186/s40562-021-00199-3
- Dickey, J. O., Bentley, C. R., Bilham, R., and Carton, J. A. (1997). *Satellite Gravity and the Geosphere: Contributions to the Study of the Solid Earth and its Fluid Envelopes* (Washington: National Acad. Press).
- Ding, Q., Steig, E. J., Battisti, D. S., and Wallace, J. M. (2012). Influence of the Tropics on the Southern Annular Mode. *J. Clim.* 25, 6330–6348. doi: 10.1175/JCLI-D-11-00523.1
- Gill, A. E., and Niiler, P. P. (1973). The Theory of the Seasonal Variability in the Ocean. *Deep. Res.* 20, 141–177. doi: 10.1016/0011-7471(73)90049-1
- Huang, R., and Jin, X. (2002). Sea Surface Elevation and Bottom Pressure Anomalies Due to Thermohaline Forcing. Part I: Isolated Perturbations. *J. Phys. Oceanogr.* 32, 2131–2150. doi: 10.1175/1520-0485(2002)032<2131:SSEABP>2.0.CO;2
- Huang, R., Jin, X., and Zhang, X. (2001). An Oceanic General Circulation Model in Pressure Coordinates. *Adv. Atmos. Sci.* 18, 18–21. doi: 10.1007/s00376-001-0001-9

- Hughes, C. W., and de Cuevas, B. A. (2001). Why Western Boundary Currents in Realistic Oceans are Inviscid: A Link Between Form Stress and Bottom Pressure Torques. *J. Phys. Oceanogr.* 31, 2871–2885. doi: 10.1175/1520-0485(2001)031<2871:WWBCIR>2.0.CO;2
- Hughes, C. W., and Smithson, M. J. (1996). Bottom Pressure Correlations in the South Atlantic. *Geophys. Res. Lett.* 23, 2243–2246. doi: 10.1029/96GL01319
- Hughes, C. W., Wunsch, C., and Zlotnicki, V. (2000). Satellite Peers Through the Oceans From Space. *Eos. (Washington, DC)* 81, 68. doi: 10.1029/00EO00046
- Jin, S. (2013). Satellite Gravimetry and Mass Transport in the Earth System. *Obs. Model. Appl.* (London). 157–174. doi: 10.5772/51698171
- Jing, X., and Cheng, X. (2019). Seasonal and Long-Term Variability of Ocean Bottom Pressure in the Indian Ocean. *J. Trop. Oceanogr.* 38, 10–17. doi: 10.11978/2018131
- Johnson, G. C., and Chambers, D. P. (2013). Ocean Bottom Pressure Seasonal Cycles and Decadal Trends From GRACE Release-05: Ocean Circulation Implications. *J. Geophys. Res. Ocean.* 118, 4228–4240. doi: 10.1002/jgrc.20307
- Kanzow, T., Flechtner, F., Chave, A., Schmidt, R., Schwintzer, P., and Send, U. (2005). Seasonal Variation of Ocean Bottom Pressure Derived From Gravity Recovery and Climate Experiment (GRACE): Local Validation and Global Patterns. *J. Geophys. Res. C. Ocean.* 110, 1–14. doi: 10.1029/2004JC002772
- Landerer, F. W., and Swenson, S. C. (2012). Accuracy of Scaled GRACE Terrestrial Water Storage Estimates. *Water Resour. Res.* 48, 1–11. doi: 10.1029/2011WR011453
- Lee, T., Hobbs, W. R., Willis, J. K., Halkides, D., Fukumori, I., Armstrong, E. M., et al. (2010). Record Warming in the South Pacific and Western Antarctica Associated With the Strong Central-Pacific El Niño in 2009–10. *Geophys. Res. Lett.* 37, 1–6. doi: 10.1029/2010GL044865
- Makowski, J. K., Chambers, D. P., and Bonin, J. A. (2015). Using Ocean Bottom Pressure From the Gravity Recovery and Climate Experiment (GRACE) to Estimate Transport Variability in the Southern Indian Ocean. *J. Geophys. Res. Ocean.* 1–16, 4245–4259. doi: 10.1002/2014JC010575. Received
- Marshall, G. J. (2003). Trends in the Southern Annular Mode From Observations and Reanalyses. *J. Clim.* 16, 4134–4143. doi: 10.1175/1520-0442(2003)016<4134:TITSAM>2.0.CO;2
- McIntosh, P. C., and Hendon, H. H. (2018). Understanding Rossby Wave Trains Forced by the Indian Ocean Dipole. *Clim. Dyn.* 50, 2783–2798. doi: 10.1007/s00382-017-3771-1
- Peralta-ferriz, C., Landerer, F. W., Chambers, D. P., Volkov, D., and Llovel, W. (2017). Remote Sensing of Bottom Pressure From GRACE Satellites. *US Clivar. Var.* 15, 22–28.
- Piecuch, C. G., and Ponte, R. M. (2014). Annual Cycle in Southern Tropical Indian Ocean Bottom Pressure. *J. Phys. Oceanogr.* 44, 1605–1613. doi: 10.1175/JPO-D-13-0277.1
- Piecuch, C. G., Quinn, K. J., and Ponte, R. M. (2013). Satellite-Derived Interannual Ocean Bottom Pressure Variability and Its Relation to Sea Level. *Geophys. Res. Lett.* 40, 3106–3110. doi: 10.1002/grl.50549
- Ponte, R. M. (1999). A Preliminary Model Study of the Large-Scale Seasonal Cycle in Bottom Pressure Over the Global Ocean. *J. Coast. Res.* 104, 1289–1300. doi: 10.1029/1998JC900028
- Ponte, R. M., and Piecuch, C. G. (2014). Interannual Bottom Pressure Signals in the Australian-Antarctic and Bellingshausen Basins. *J. Phys. Oceanogr.* 44, 1456–1465. doi: 10.1175/JPO-D-13-0223.1
- Price, J. F., Weller, R. A., and Schudlich, R. R. (1987). Wind-Driven Ocean Currents and Ekman Transport. *Science* 238, 1534–1538. doi: 10.1126/science.238.4833.1534
- Qin, J., Cheng, X., Yang, C., Ou, N., and Xiong, X. (2022). Mechanism of Interannual Variability of Ocean Bottom Pressure in the South Pacific. *Clim. Dyn.* doi: 10.1007/s00382-022-06198-0
- Rintoul, S. R. (2018). The Global Influence of Localized Dynamics in the Southern Ocean. *Nature* 558, 209–218. doi: 10.1038/s41586-018-0182-3
- Tapley, B. D., Bettadpur, S., Watkins, M., and Reigber, C. (2004). The Gravity Recovery and Climate Experiment: Mission Overview and Early Results. *Geophys. Res. Lett.* 31, 1–4. doi: 10.1029/2004GL019920
- Tapley, B. D., Watkins, M. M., Flechtner, F., Reigber, C., Bettadpur, S., Rodell, M., et al. (2019). Contributions of GRACE to Understanding Climate Change. *Nat. Clim. Change* 9, 358–369. doi: 10.1038/s41558-019-0456-2
- Taschetto, A. S., Gupta, A. S., Hendon, H. H., Ummenhofer, C. C., and England, M. H. (2011). The Contribution of Indian Ocean Sea Surface Temperature Anomalies on Australian Summer Rainfall During EL Niño Events. *J. Clim.* 24, 3734–3747. doi: 10.1175/2011JCLI3885.1
- Woodworth, P. L., Vassie, J. M., Hughes, C. W., and Meredith, M. P. (1996). A Test of the Ability of TOPEX/POSEIDON to Monitor Flows Through the Drake Passage. *J. Geophys. Res. C. Ocean.* 101, 11935–11947. doi: 10.1029/96JC00350
- Yeh, S. W., Kug, J. S., Dewitte, B., Kwon, M. H., Kirtman, B. P., and Jin, F. F. (2009). El Niño in a Changing Climate. *Nature* 461, 511–514. doi: 10.1038/nature08316
- Zhang, Y., Lin, Y. H., and Huang, R. X. (2014). A Climatic Dataset of Ocean Vertical Turbulent Mixing Coefficient Based on Real Energy Sources. *Sci. China Earth Sci.* 57, 2435–2446. doi: 10.1007/s11430-014-4904-6

**Conflict of Interest:** The authors declare that the research was conducted in the absence of any commercial or financial relationships that could be construed as a potential conflict of interest.

**Publisher's Note:** All claims expressed in this article are solely those of the authors and do not necessarily represent those of their affiliated organizations, or those of the publisher, the editors and the reviewers. Any product that may be evaluated in this article, or claim that may be made by its manufacturer, is not guaranteed or endorsed by the publisher.

Copyright © 2022 Niu, Cheng, Qin, Ou, Yang and Huang. This is an open-access article distributed under the terms of the Creative Commons Attribution License (CC BY). The use, distribution or reproduction in other forums is permitted, provided the original author(s) and the copyright owner(s) are credited and that the original publication in this journal is cited, in accordance with accepted academic practice. No use, distribution or reproduction is permitted which does not comply with these terms.